ANALYSIS OF LARGE SCALE TESTS FOR AP-600 PASSIVE CONTAINMENT COOLING SYSTEM*

by

W. T. Sha, T. H. Chien, J. G. Sun, and B. T. Chao

Energy Technology Division
Argonne National Laboratory
Argonne, Illinois 60439

DISCLAIMER

Submitted to the Second International Topical Meeting on Advanced Reactor Safety (ARS '97)

*This work was sponsored by Division of System Research, The Office of Nuclear Regulatory Research, U.S. Nuclear Regulatory Commission

ANALYSIS OF LARGE SCALE TESTS FOR AP-600 PASSIVE CONTAINMENT COOLING SYSTEM

W. T. Sha
ANL-E
ET-308
Argonne, IL 60439
(630) 252-5910

T. H. Chien
ANL-E
ET-308
Argonne, IL 60439
(630) 252-8462

J. G. Sun
ANL-E
ET-212
Argonne, IL 60439
(630) 252-5169

B. T. Chao
Dept of Mech. Eng.
Univ. of IL-Urbana
Urbana, IL 61801

ABSTRACT: *All next-generation light water reactors utilize passive systems to remove heat via natural circulation and are significantly different from past and current nuclear plant designs. One unique feature of the AP-600 is its passive containment cooling system (PCCS), which is designed to maintain containment pressure below the design limit for 72 hours without action by the reactor operator. During a design-basis accident, i.e., either a loss-of-coolant or a main steam-line break accident, steam escapes and comes in contact with the much cooler containment vessel wall. Heat is transferred to the inside surface of the steel containment wall by convection and condensation of steam and through the containment steel wall by conduction. Heat is then transferred from the outside of the containment surface by heating and evaporation of a thin liquid film that is formed by applying water at the top of the containment vessel dome. Air in the annular space is heated by both convection and injection of steam from the evaporating liquid film. The heated air and vapor rise as a result of natural circulation and exit the shield building through the outlets above the containment shell. All of the analytical models that are developed for and used in the COMMIX-1D code for predicting performance of the PCCS will be described. These models cover governing conservation equations for multicomponents single phase flow, transport equations for the k-ε two-equation turbulence model, auxiliary equations, liquid-film tracking model for both inside (condensate) and outside (evaporating liquid film) surfaces of the containment vessel wall, thermal coupling between flow domains inside and outside the containment vessel, and heat and mass transfer models. Various key parameters of the COMMIX-1D results and corresponding AP-600 PCCS experimental data are compared and the agreement is good. Significant findings from this study are summarized.*

I. INTRODUCTION

The AP-600, an advanced pressurized-water reactor, utilizes a passive containment cooling system (PCCS) to remove heat released inside the containment vessel following postulated design-basis accidents (DBA) such as a loss of coolant accident (LOCA) or a main steam-line break (MSLB). During a DBA, heat released to the interior of the steel containment vessel is removed by evaporation of a continuously flowing thin liquid film on the outside surface of the vessel, which lowers the temperature of the steel vessel wall so that steam condenses on its inside surface. Consequently, the pressure of the gaseous mixture inside the containment vessel is lowered and so is its temperature. The thin liquid film outside the steel vessel wall is formed by applying water at the top of the ellipsoidal containment dome. Evaporation of the falling liquid film is enhanced by buoyancy-driven flows of moist air in an annular space between the outside of the steel containment shell wall and the inside a baffle suspended from the shield building wall. Air inlets are provided at the top of the shield building. The AP-600 PCCS is designed to maintain containment pressure below the design limit for 72 hours without operator action during a DBA. A schematic sketch of the PCCS is shown in Fig. 1. The objectives of this paper are to (a) describe the models used in the latest developmental version of COMMIX family code [1-4], i.e. COMMIX-1D [5] for predicting the PCCS performance; (b) compare the predicted results obtained from COMMIX-1D with a selected set of the Westinghouse's AP-600 PCCS large-scale tests (LSTs); and (c) to summarize significant findings from this study.

II. DESCRIPTION OF ANALYTICAL MODEL USED IN COMMIX-1D FOR PREDICTING PCCS PERFORMANCE

Because the PCCS uses condensation and evaporation, an analytical model for predicting PCCS performance must apparently consider two-phase flow. After careful examination of the physical behavior, and judicious selection of computational domains in the PCCS, we found that the analytical model used in the COMMIX-1D code [5] can be greatly simplified from formulation of two-phase flow to single-phase flow with multi- components. The PCCS is divided into three domains, namely a bulk gaseous mixture inside the containment vessel is denoted as domain 1, bulk moist air in an annulus between the outside containment shell and the inside shielding building wall is denoted as domain 2 and a thermal coupling domain linking domains 1 and 2 is named as domain 3. The thermal coupling domain consists of condensate film inside the

containment vessel wall, the containment vessel wall itself, evaporating liquid film outside the containment vessel wall, and paint on both sides of the vessel wall.

In the analytical model, we further assume that (a) the volume occupied by the thin liquid film in domain 1 or 2 is very small relative to the corresponding volume of domain 1 or 2 and can be neglected without affecting overall results, and (b) both the evaporation and condensation rate at the interface between the liquid film and the bulk gaseous mixture can be computed iteratively and treated as boundary conditions for domains 1 and 2. The analytical model used in the COMMIX-1D [5] code for predicting PCCS performance has been developed and its details are presented below.

A. Governing Conservation Equations for Multicomponents Single Phase Flow

The three–dimensional time–dependent conservation equations of mass, momentum, and energy for a mixture of N components, based on the porous–medium formulation through local volume averaging [6] are

Mixture continuity equation

$$\gamma_v \frac{\partial \rho}{\partial t} + \nabla \cdot (\gamma_A \rho \bar{v}) = \gamma_v \dot{m}, \qquad (2.1)$$

Component continuity equation

$$\gamma_v \frac{\partial}{\partial t}(\rho x_k) + \nabla \cdot (\gamma_A x_k \rho \bar{v})$$

$$= \gamma_v \dot{m}_k + \nabla \cdot (\gamma_A \rho D_{k,eff} \nabla x_k), \qquad (2.2)$$

Mixture momentum equation

$$\gamma_v \frac{\partial}{\partial t}(\rho \bar{v}) + \nabla \cdot (\gamma_A \rho \bar{v}\bar{v}) = -\gamma_v \nabla p$$

$$+\nabla \bullet (\gamma_A \mu_{eff} \nabla \bar{v}) + \gamma_v \rho \bar{g} \qquad (2.3)$$

$$-\gamma_v \bar{R} + \sum_{k=1}^{N} \dot{m}_k \bar{v}_{sk},$$

Mixture energy equation

$$\gamma_v \frac{\partial}{\partial t}(\rho h) + \nabla \bullet (\gamma_A \rho \bar{v} h) = \gamma_v \frac{dp}{dt} +$$

$$\nabla \bullet (\gamma_A k_{eff} \nabla T) + \gamma_v \sum_{k=1}^{N} \dot{m}_k h_{sk} + \gamma_v \dot{Q}_s$$

$$+ \sum_{k=1}^{N} \nabla \bullet \left[(\gamma_A \rho D_{k,eff} \nabla (x_k h_k) \right], \qquad (2.4)$$

where:

k = 1, 2, ..., N, component in a mixture,
k_{eff} = $k_m + k_t$ = effective thermal conductivity of mixture, W/m/°C,
k_m = molecular thermal conductivity of mixture, W/m/°C,
k_t = turbulent thermal conductivity of mixture, W/m/°C,
ρ = mixture density, kg/m^3,
γ_A = surface porosity,
γ_v = volume porosity,
x_k = mass fraction for component k, $\Sigma x_k = 1$,
$\dot{m}_k$ = mass source for component k, kg/m^3/s,
$\dot{m}$ = $\Sigma \dot{m}_k$,
$\bar{v}$ = mixture velocity, m/s,
$\bar{v}_{sk}$ = velocity associated with mass source of component k, m/s,
p = mixture pressure, Pa,
$\bar{g}$ = gravitational constant, m/s^2
h = mixture entalpy, J/kg,
h_{sk} = enthalpy associated with mass source of component k, J/kg,
Q_s = energy source, including internal heat generation and heat liberated from solid structures per unit fluid volume, W/m^3,
T = mixture temperature, °C,
μ_{eff} = $\mu_m + \mu_t$ = effective viscosity of mixture, kg/m/s,
μ_m = molecular viscosity of mixture, kg/m/s,
μ_t = turbulent viscosity of mixture, kg/m/s,
$D_{k,eff}$ = $D_{k,m} + D_{k,t}$ = effective diffusivity for component k in the mixture, m^2/s,
$D_{k,m}$ = molecular diffusivity for component k in mixture, m^2/s,
$D_{k,t}$ = turbulent diffusivity for component k in mixture, m^2/s,
$\bar{R}$ = distributed resistance per unit volume, N/m^3, and
N = total number of components in mixture.

In Eqs. 2.1–2.4, all components in the mixture are assumed to have the same velocity and temperature, and they are generally applicable for either liquid or gas systems. For containment applications, all fluid components are gases, and the formulations for the auxiliary equations, including the state equations, are based on gas systems. Furthermore, under typical containment operation and design basis accident

conditions, all gases may be treated approximately as ideal gases in the formulation for mixture quantities, while for evaluating a single-component property for steam, more rigorous correlation functions are used in the code.

B. Transport Equations for k-ε Two-Equation Turbulence Model [7,8]

Transport Equation for Turbulence Kinetic Energy, k

$$\rho\frac{\partial k}{\partial t}+\rho u_j\frac{\partial k}{\partial x_j}=P_k+G_k-\rho\varepsilon$$

$$+\frac{\partial}{\partial x_j}\left[\left(\frac{\mu_t}{\sigma_k}+\mu_m\right)\frac{\partial k}{\partial x_j}\right], \qquad (2.5)$$

where:

$$P_k=\mu_t\left[\frac{\partial u_i}{\partial x_j}\left(\frac{\partial u_i}{\partial x_j}+\frac{\partial u_j}{\partial x_i}\right)\right] \qquad (2.6)$$

is the source due to mean shear, and

$$G_k=-\frac{\mu_t}{\rho\sigma_h}\frac{\partial\rho}{\partial T}\left(\frac{\partial T}{\partial x_j}g_j\right) \qquad (2.7)$$

is the source due to thermal buoyancy, where σ_h is the turbulent Prandtl number for the energy equation and has a recommended value of 0.9. The term containing σ_k in Eq. 2.5 represents the diffusion of k. σ_k is called the turbulent Prandtl number for k. Launder et al. [9] have recommended the value 1.0 for σ_k.

Transport Equation for Dissipation of k, ε

$$\rho\frac{\partial\varepsilon}{\partial t}+\rho u_j\frac{\partial\varepsilon}{\partial x_j}=C_1\frac{\varepsilon}{k}(P_k+G_k)$$

$$-C_2\frac{\rho\varepsilon^2}{k}+\frac{\partial}{\partial x_j}\left[\left(\frac{\mu_t}{\sigma_\varepsilon}+\mu_m\right)\frac{\partial\varepsilon}{\partial x_j}\right]. \qquad (2.8)$$

Here, the source terms P_k and G_k have the same form as in Eqs. 2.6 and 2.7, respectively; the second term on the right is the dissipation term; and the last term represents diffusion. The variable σ_ε is the turbulent Prandtl number for ε; the recommended value [10] is 1.3. The coefficient of the production term C_1 is normally chosen by reference to near-wall turbulence, whereas the coefficient C_2 is determined from the decay of grid turbulence. The values of C_1 and C_2 recommended by Launder et al. [11] are 1.44 and 1.92, respectively.

C. Auxiliary Equations

1. Turbulent Transport Properties

Turbulent Viscosity μ_t

The turbulent viscosity for a single phase is normally computed on the basis of the turbulence model used. In the k–ε two-equation turbulence model as outlined above, turbulent viscosity is calculated from

$$\mu_t=\frac{C_D\rho k^2}{\varepsilon} \qquad (2.9)$$

where C_D is a constant having a recommended value of 0.09.

Turbulent Thermal Conductivity k_t

The turbulent thermal conductivity of a mixture is defined as

$$k_t=\frac{C_p\mu_t}{\sigma_h}, \qquad (2.10)$$

where C_p is the mixture specific heat.

Turbulent Diffusivity $D_{k,t}$

The turbulent diffusivity of a mixture $D_{k,t}$ is defined as

$$D_{k,t}=\frac{\mu_t}{\rho Sc}, \qquad (2.11)$$

where Sc is the Schmidt number having a recommended value of 0.75.

2. Mass Source $\dot{m}_k$ and Associated Velocity $\bar{v}_{sk}$ and Enthalpy h_{sk}

In containment systems, only the steam component in the gas mixture gives rise to a mass source term through condensation and evaporation. If we denote $\dot{m}_c$ and $\dot{m}_e$ as the steam condensation mass flux and water evaporation mass flux in the system, respectively, and they are positive and have a unit of kg/m^2 /s. The mass source term in the mixture continuity Eq. 2.1 and in the component continuity Eq. 2.2 are related to these mass fluxes. For passive containment cooling system, such as employed in AP-600 as shown in Fig. 1, mass source term can be written as;

$$\sum_{k=1}^{N}\dot{m}_k=\dot{m}=A(\dot{m}_e-\dot{m}_c), \qquad (2.12)$$

With understanding that $\dot{m}_e$ equals to zero inside the containment vessel, and $\dot{m}_c$ equals to zero in exterior air annulus.

In Eq. 2.12, A is the heat transfer area per unit volume. The formulations for the condensation flux $\dot{m}_c$ and evaporation flux $\dot{m}_e$ will be presented in Eqs. 2.38a and 2.38b.

The momentum source term in the mixture momentum Eq. 2.3 is evaluated as

$$\sum_{k=1}^{N} \dot{m}_k \bar{v}_{sk} = A(\dot{m}_e - \dot{m}_c)\bar{v} \qquad (2.13)$$

where $\bar{v}$ is the mixture velocity.

The energy source term in the mixture energy Eq. 2.4 is evaluated as

$$\sum_{k=1}^{N} \dot{m}_k h_{sk} = A[\dot{m}_e h_g(T_{if}, p_{vi}) - \dot{m}_c h_g(T, p_{vb})], \qquad (2.14)$$

where h_g is the enthalpy of the steam and is evaluated at the mixture/liquid interface temperature T_{if} and pressure p_{vi} (at saturation condition) for the evaporation steam source, and at the bulk mixture temperature T and pressure p_{vb} for the condensation steam sink.

In COMMIX–1D, both condensation and evaporation are modeled for the containment vessel wall surfaces in the liquid–film tracking models [12, 13]. Steam condensation on the internal thermal structures can also be accounted for. However, because COMMIX–1D does not compute liquid water distribution inside the containment vessel except on the vessel wall, water evaporation from internal thermal structures is not allowed in the code.

D. Liquid-Film Tracking Model

Two liquid–film tracking models for time–dependent flows (a simplified model and a comprehensive model) have been developed and implemented in the COMMIX–1D code. They can be used to predict both the evaporating film on the outside surface of the vessel and the condensate film on its inside. Filmwise condensation is assumed inside the containment vessel wall. The tracking models compute the liquid–film thickness, its mean velocity, and its temperature on both sides of the steel containment vessel.

In both models, a differential equation describing the time rate of change of the film thickness is rigorously derived from first principles. This equation relates the time rate of thickness change to the streamwise gradient of the mass flow rate and the condensate mass flux at the film's free surface. In the simplified model, the inertia terms in the momentum equation were ignored to obtain an explicit expression of the velocity field in the film. Arguments will be given in Section IV, Discussion and Conclusions to show that the simplification could be justified except for brief times following a disturbance.

In the comprehensive model, the inertia terms were retained in the momentum equation, and a parabolic velocity distribution was assumed across the film thickness. In both models, linear temperature distributions across the film thickness were assumed in the energy equation. For all practical purposes, both models give essentially the same results.

Governing Equations, Boundary Conditions, and Liquid/Vapor Interfacial Conditions

Experimental observations indicated that the liquid films developed on the containment vessel walls are usually very thin, on the order of a few tenths of a millimeter. At the containment design conditions, the Reynolds numbers of these films are expected to be well within the laminar flow regime. Based on these observations, the laminar–boundary–layer type of analysis is used for the development of the liquid–film tracking models.

The dynamic equations for steady, axisymmetrical, boundary–layer flow over a body of revolution were first given by E. Boltz [12] and are most conveniently expressed in orthogonal curvilinear coordinates (see Ref. 13). As seen in Fig. 2, x is the distance measured along a meridian from the stagnation point S. The coordinate y is normal to x and points inward for analysis of condensate film flow on the inside surface and outward for analysis of evaporating water film on the exterior. The body contour is specified by the radius r(x) of the section perpendicular to the axis of symmetry. The contour has no sharp corners so that $d^2\ r/dx^2$ is continuous everywhere. The velocity components along the x– and y–directions are denoted by u and v, respectively. The gravitational acceleration vector $\bar{g}$ is colinear with the axis of rotational symmetry as illustrated, and the angle between $\bar{g}$ and x is β. The condensate flows along the undersurface of the dome and then down the vertical wall of the cylinder shell, mainly due to gravity, and is resisted by fluid viscosity. The pressure gradient in the streamwise direction is assumed to be low relative to the gravitational and viscous forces. Because the

temperature difference across the film is small, all properties are considered constant in the derivation. The same can be said for the flow of the evaporating water film on the outside. The condensate flow rate increases with x from the stagnation point S, with a continuous increase in resistance to heat transfer along the vertical cylindrical wall. The water film on the outside evaporates such that its flow rate decreases with x with a corresponding change in heat transfer coefficient.

The time–dependent conservation equations are

Mass:

$$\frac{\partial(ru)}{\partial x} + \frac{\partial(rv)}{\partial y} = 0. \qquad (2.15)$$

To be consistent with boundary–layer approximation, r is regarded as a function of x only, and hence the second term can be written as $r\partial v/\partial y$.

Momentum:

$$\rho\left(\frac{\partial u}{\partial t} + u\frac{\partial u}{\partial x} + v\frac{\partial u}{\partial y}\right) = \mu\frac{\partial^2 u}{\partial y^2} + \rho g\cos\beta \qquad (2.16)$$

Energy:

$$\rho C_p\left(\frac{\partial T}{\partial t} + u\frac{\partial T}{\partial x} + v\frac{\partial T}{\partial y}\right) = k\frac{\partial^2 T}{\partial y^2}. \qquad (2.17)$$

In Eq. 2.16, μ and ρ are the viscosity and density of the liquid film, respectively. In Eq. 2.17, T is the temperature and k and C_p are the thermal conductivity and specific heat of the liquid, respectively.

The boundary conditions are

At the wall, y = 0:

$$u = v = 0, \quad T = T_w, \qquad (2.18a,b)$$

At the liquid/vapor interface, $y = \delta(t,x)$:

$$\frac{\partial u}{\partial y} = 0, \qquad (2.19a)$$

$$\rho\frac{\partial \delta}{\partial t} - \rho v + \rho u\frac{\partial \delta}{\partial x} = \dot{m}_c, \qquad (2.19b)$$

$$k\frac{\partial T}{\partial y} = \dot{m}_c h_{fg} + h_c(T_b - T_{if}). \qquad (2.19c)$$

In Eq. 2.18b, T_w is the local temperature on the wall surface. The film thickness δ is a function of time and meridian distance. The condition $\partial u/\partial y = 0$ implies that interfacial shear is negligible. Equation 2.19b is the interfacial kinematic relation, with $\dot{m}_c$ being the condensate mass flux. Equation 2.19c is the interfacial heat balance relation in which h_{fg} is the enthalpy of condensation. The second term on the right side of Eq. 2.19c accounts for the convective heat flux resulting from the bulk motion of the vapor/air mixture in the containment vessel. It is expressed in terms of convective heat transfer coefficient h_c and a temperature difference $(T_b - T_{if})$; here, T_b is the bulk temperature of the local vapor/air mixture, and T_{if} is the local interfacial temperature, which is taken to be the saturation temperature corresponding to the partial pressure of the vapor at the interface. If T_b is superheated, h_{fg} is computed according to $h_g(T_b) - h_f(T_{if})$, where $h_g(T_b)$ is the enthalpy of the bulk mixture at superheated temperature T_b, and $h_f(T_{if})$ is the enthalpy of the saturated liquid at interface temperature T_{if}.

The initial condition is simply

$$\delta(t = 0,x) = 0. \qquad (2.20)$$

In passing, we note that the well–known Nusselt's film condensation analysis for a flat plate is for steady flow and neglects convective transport in both the momentum equation and the energy equation. Consequently, Eq. 2.16 is reduced to

$$\mu\frac{\partial^2 u}{\partial y^2} + \rho g\cos\beta = 0, \qquad (2.21)$$

and Eq. 3.3 is reduced to

$$k\frac{\partial^2 T}{\partial y^2} = 0. \qquad (2.22)$$

Integration of Eq. 2.21 yields a parabolic profile with maximum occurring at $y = \delta$. Equation 2.22 leads to a linear temperature distribution across the film.

In domain 2 where only evaporation occurs, it is necessary to replace $\dot{m}_c$ in Eqs. 2.19b and Eq. 2.19c by $-\dot{m}_e$. Clearly in this case T_b is lower than T_{if}.

E. Thermal Coupling between Flow Domains inside and outside the Containment Vessel

In the PCCS analysis, the flow domains inside and outside the containment vessel are separated by the containment steel shell. The only coupling between them is the thermal coupling by the heat transfer through the shell. Various heat transfer mechanisms are considered, including those at the boundaries that separate the gaseous mixture inside the vessel, the condensate film, the paint on the inside wall, the shell wall, the paint on the outside shell wall, the evaporating liquid film, and the

moist air in the annulus. In the analysis that follows, it is assumed that heat flow is predominantly in the radial direction (perpendicular to the vessel wall) except for the liquid films, for which convection parallel to the surface is also considered. Figure 3 illustrates the discretization scheme of the thermal structure currently used in the COMMIX-1D code for AP-600 PCCS applications. The wall of the steel shell can be divided into a number of computational cells. The radial length of cell j is Δr_j and the total cell number is L. When j = 1, the volume element or cell represents the condensate film, and when j = L, it represents the evaporating liquid film. The finite-difference energy equation governing the temperature field in the radial direction at a given axial length Δx along the meridian direction (x) from level k-1 to level k can be written as

$$\frac{\rho_j C_{pj} V_j}{\Delta t}\left(T_j - T_j^{\,n}\right) = q_j - q_{j+1} + \left[\left(m_{fj} C_{pj} T_j\right)_{k-1} - \left(m_{fj} C_{pj} T_j\right)_k\right] \delta_{jM} + Q_j''' V_j \qquad (2.23)$$

$j = 1, 2...L$
$M = 1$ or L
$\delta_{jM} = 1$ only $j = M$
$\delta_{jM} = 0 \qquad j \neq M,$

where:

ρ = density,
C_p = specific heat,
T = temperature,
Δt = time increment,
q = heat flow rate across radial surfaces of computational cell,
V = cell volume,
Q''' = volumetric heat source, and
m_f = film mass flow rate in x direction.

Superscript n refers to the previous time step.

When j = 1

$$q_1 = q_{conv,1} + \dot{m}_c A_1 h_g \qquad (2.24)$$

with

$$q_{conv,1} = h_1 A_1 \left(T_i - T_{ii}\right) \qquad (2.25)$$

and

$$q_2 = U_2 A_2 \left(T_1 - T_2\right) \qquad (2.26)$$

with

$$U_2 = \frac{1}{\frac{\Delta r_1}{2k_1} + \frac{\Delta r_2}{2k_2}}. \qquad (2.27)$$

In the foregoing equations, $q_{conv,1}$ is the convective heat transfer rate at A_1 that is the result of the difference in the temperature of the vapor/air mixture inside the vessel and that of the surface of the condensate film. Thus, in Eq. 2.25, h_1 is a heat transfer coefficient due to convection, T_i is the bulk temperature of the vapor/air mixture adjacent to A_1, and T_{ii} is temperature of the condensate-film surface. The first subscript i denotes inside, and the second subscript i denotes interface. At the surface A_1, there is a vapor mass flux equal to $\dot{m}_c$ entering the control volume inasmuch as air is non-condensable. This vapor flow carries with it a specific enthalpy h_g, which is the saturation enthalpy corresponding to the interface temperature T_{ii}. In Eq. 2.24, $\dot{m}_c A_1 h_g$ denotes the enthalpy flow rate into the control volume due to mass transfer as a result of condensation. The conduction heat transfer rate q_2 through surface A_2 is given by Eq. 2.26, in which U_2 is defined by Eq. 2.27, where k_1 is the thermal conductivity of liquid film, k_2 is the thermal conductivity of paint, Δr_1 is the liquid-film thickness, and Δr_2 is the thickness of the inside paint coating. The mass inflow rate of the condensate film at the upper surface of the control volume is $(m_{fl})_{k-1}$ and its outflow rate at the lower surface is $(m_{fl})_k$.

When j = 2,3,...., L-1

$$q_j = U_j A_j \left(T_{j-1} - T_j\right), \qquad (2.28)$$

$$q_{j+1} = U_{j+1} A_{j+1} \left(T_j - T_{j+1}\right), \qquad (2.29)$$

$$U_j = \frac{1}{\frac{\Delta r_{j-1}}{2k_{j-1}} + \frac{\Delta r_j}{2k_j}}. \qquad (2.30)$$

and

$$U_{j+1} = \frac{1}{\frac{\Delta r_j}{2kj} + \frac{\Delta r_{j+1}}{2k_{j+1}}}. \qquad (2.31)$$

In these equations, q_j and q_{j+1} are the conduction heat flow rate across surfaces A_j and A_{j+1}, respectively, and U_j and U_{j+1} are the equivalent heat transfer coefficients.

When j = L

$$q_L = U_L A_L (T_{L-1} - T_L), \qquad (2.32)$$

$$U_L = \frac{1}{\frac{\Delta r_{L-1}}{2k_{L-1}} + \frac{\Delta r_L}{2k_L}}, \text{ and} \qquad (2.33)$$

$$q_{L+1} = q_{conv,L+1} + \dot{m}_e A_{L+1} h_g, \qquad (2.34)$$

with

$$q_{conv,L+1} = h_{L+1} A_{L+1} (T_{oi} - T_o), \qquad (2.35)$$

In the foregoing equations, q_L is the conduction heat flow rate through surface A_L, and q_{L+1} is the total heat transfer rate through surface A_{L+1}. q_{L+1} has two components: $q_{conv,L+1}$ the heat transfer due to convection, and $\dot{m}_c A_{L+1} h_g$ is the enthalpy outflow rate from the control volume due to evaporation at the surface of the liquid film. In Eq. 2.35, $q_{conv,L+1}$ is expressed in terms of heat transfer coefficient h_{L+1} and a temperature difference (T_{oi} - T_o), where T_{oi} is the surface temperature of the evaporating film, and T_o is the bulk temperature of the air/vapor mixture adjacent to A_{L+1} in the annulus; $\dot{m}_c$ is the evaporation rate per unit interfacial area at A_{L+1}, and h_g is the saturation enthalpy of the vapor corresponding to T_{oi}.

F. Heat and Mass Transfer Models

Solutions of the energy equation as described in the previous section would require information on the local convective heat-transfer coefficient h_1 in Eq. 2.25 between the bulk of the gaseous mixture flow inside the vessel and the free surface of the condensate film, as well as the h_{L+1} in Eq. 2.35 between the free surface of the evaporating film and the bulk of the moist air flow in the annulus outside the vessel. Judging from the large height of the system, one would expect that buoyancy plays an important role. The heat and mass transfer models used in the CONTAIN code [14] are described in the next two sections, respectively, and are implemented in the COMMIX-1D code. A preliminary turbulent mixed-convection (TMC) model [15] used in the COMMIX-1D code is then described.

1. Heat-transfer Models Used in CONTAIN Code

Several correlations for the Nusselt number [$Nu=h_cL/k$] were used in CONTAIN [14]. The characteristic length L in Nu is chosen on the basis of the problem under investigation. The convective heat-transfer coefficient h_c is then used in conjunction with a temperature difference ΔT to calculate the convective heat flux to or from the vapor-gas mixture-liquid interface or the dry wall surface. Thus the heat flux is

$$q = h_c (T_b - T_i), \qquad (2.36)$$

where T_b is the fluid bulk temperature and T_i is either the vapor-gas mixture-liquid interface temperature or the dry wall temperature. The correlations follow.

For laminar natural convection:

$$h_c = \frac{k}{L}\left[0.27(Gr\,Pr)^{1/4}\right]. \qquad (2.37a)$$

For turbulent natural convection:

$$h_c = \frac{k}{L}\left[0.14(Gr\,Pr)^{1/3}\right]. \qquad (2.37b)$$

For turbulent forced convection:

$$h_c = \frac{k}{L}\left[0.037\,Re^{4/5}\,Pr^{1/3}\right]. \qquad (2.37c)$$

In the preceding equations, Pr is the Prandtl number, and the characteristic length in the Grashof number (Gr) and in the Reynolds number (Re) is also L.

2. Mass Transfer Models

A small quantity of noncondensable gas in the vapor would have a great effect on the condensation rate. The noncondensable gas will accumulate at the vapor liquid interface and thus increase the partial pressure of the gas at the interface with a simultaneous reduction of the partial pressure of the vapor because the sum of the two remains constant. The mass transport of the vapor gas mixture consists of vapor diffusion toward the interface and gas diffusion away from the interface in addition to the bulk convection of the mixture. The interface temperature (T_i) is taken to be the saturation temperature corresponding to the vapor partial pressure (p_{vi}) at the interface. If p_{vb} denotes the partial pressure of the vapor in the bulk mixture, then the mass flux of vapor at the interface is

$$\dot{m}_c = K_g \rho_{vb} \frac{p_T}{p_{vb}} \ln \frac{p_T - p_{vi}}{p_T - p_{vb}} \qquad (2.38a)$$

$$\dot{m}_e = K_g \rho_{vb} \frac{p_T}{p_{vb}} \ln \frac{p_T - p_{vb}}{p_T - p_{vi}} \qquad (2.38b)$$

where K_g is the mass transfer coefficient (having the dimension of velocity), ρ_{vb} is the mixture density, and p_T is the total system pressure. If one stipulates that heat and mass transfer processes are analogous, then

$$K_g = \frac{h_c}{C_p \rho}\left(\frac{Pr}{Sc}\right)^{2/3}. \qquad (2.39)$$

3. Turbulent-Mixed-Convection Model [15]

In mixed convection, the relative importance of the natural- and forced-convection components can be estimated by the ratio Gr_x/Re^2_x, where Gr_x is the local Grashof number and Re_x is the local Reynolds number. A commonly used rule is that when $Gr_x/Re^2_x = O(1)$, the two components are of equal importance. The forced-convection effect will dominate when $Gr_x/Re^2_x << 1$, and the natural-convection effect will dominate when $Gr_x/Re^2_x >> 1$. By examining the ratio along the vessel wall surface under the test conditions, it was found that the ratio is, in general, small near the stagnant point on the upper dome and becomes larger on the lower portion of the cylinder and the lower dome. Therefore, because of the large range of Gr_x/Re^2_x involved, a heat-transfer correlation valid for the entire mixed-convection regime is needed. For simplicity, TMC is assumed to be valid along the entire vessel wall.

An analysis of TMC along a vertical isothermal plate in aiding flow has been reported by Chen et al. [15]. The analysis employed a modified Van Driest mixing-length model for turbulent diffusivities that accounts for the buoyancy effect. On the basis of the numerical results of the analysis, they proposed the following correlation for the local Nusselt number [$Nu_x=h_cx/k$]:

$$Nu_x\, Re_x^{-0.8} = F(Pr)\left\{1 + 0.36\left[\frac{G(Pr)}{F(Pr)}\left(Gr_x / Re_x^{2.4}\right)^{1/3}\right]^3\right\}^{1/3}, \qquad (2.40)$$

where $Re_x = u_e x/\upsilon$

$Gr_x = g\beta\Delta T x^3/\upsilon^2$

$F(Pr) = 0.0287 Pr^{0.6}$

$G(Pr) = 0.150 Pr^{1/3}\left[1 + (0.492/Pr)^{9/16}\right]^{-16/27}$

As noted in Ref. 15, Eq. 2.40 converges to the known result for pure turbulent forced convection over a vertical plate when $Gr_x/Re_x^2 \to 0$; however, it underpredicts the local Nusselt number by about 29% in the pure free convection limit when $Gr_x/Re_x^2 \to \infty$. Chen et al. [15] also noted that in the free-convection-dominated regime, a better correlation was obtained by replacing the numerical constant 0.36 by 0.52. Pending future analysis of additional PCCS experimental data, the following heat-transfer correlation for TMC is tentatively proposed for this study:

$$Nu_x = C Re_x^{4/5} F(Pr)\left\{1 + \alpha\left[\frac{G(Pr)}{F(Pr)}\left(Gr_x / Re_x^{2.4}\right)^{1/3}\right]^3\right\}^{1/3} \qquad (2.41)$$

where C = 1.4 to account for the fluctuating condensate surface

$$\alpha = \begin{cases} 0.36 \text{ for } Gr_x/Re_x^2 < 1 \\ 0.52 \text{ for } Gr_x/Re_x^2 \geq 1 \end{cases}$$

III. NUMERICAL RESULTS AND THEIR COMPARISON WITH EXPERIMENTAL DATA OF LARGE-SCALE TESTs (LSTs)

A. Numerical Model Used in COMMIX-1D Code

A cylindrical coordinate (R, θ, z) is used in the COMMIX-1D code for numerical simulation of Westinghouse's AP-600 PCCS Large-Scale Tests, and 180° symmetry in R-θ plane is assumed in the numerical model. Figures 4 and 5 are computational mesh setups for LSTs in R-Z and R-θ cross sections, respectively. I, J, and K are computational mesh indices in the radial (R), circumferential (θ) and axial (Z) directions respectively. Judicious selection of computational mesh size and location is based on the physical arrangement of structures of LSTs as well as on a balance between accuracy of the numerical results and computer running time. Based on experimental observation, dry strips are generally formed from the top of dome down to the bottom of cylinder with the same circumferential angle. We assume that all dry strips can be lumped into one circumferential sector. This assumption will result in a slightly higher containment pressure, which is conservative from a reactor safety standpoint. Westinghouse's 1/8-Scale Test Facility for AP-600 PCCS Large Scale Tests is very similar as shown in Fig. 1, with some simplifications on internal components and structures.

B. Description of LST

The experimental data used in the comparison of numerical results obtained from COMMIX-1D code are prototypical LSTs of 1/8-scale. A brief description of the selected set of LSTs [17] is given below:

Tests 1 and 2 were steam-flow-rate-specific tests without dry strips (patches) (i.e., 100% water coverage) over the outside surface of the containment vessel. The effects of the various parameters were investigated by changing the steam flow rate while other parameters were held constant. Test 2 has much larger steam flow rate than

Test 1. The steam flow rate used in all LSTs is intended to simulate the break flow rate in a postulated accident.

Tests 3 and 4 were conducted mainly to study the effects of the various water coverages over the outside surface of the containment vessel. Test 4 has a lower steam flow rate than Test 3. Many more dry strips over the outside surface of containment vessel were observed experimentally in Test 3 and Test 4.

Tests 5 and 6 were performed where air flow was allowed to develop in natural convection (prior to initiation of the forced draft fan) to force convection flow in the air annulus. The steam flow rate was held approximately constant throughout the tests. After steady-state conditions were reached (Test 5 corresponds to this steady-state condition), the fan was activated and kept on until another steady-state condition was reached following the transient caused by the fan. (Test 6 corresponds to this steady-state condition including the portion of transient). The purpose of Tests 5 and 6 is to validate the computer code's ability to model the transition from free convection to forced convection in the air annulus.

Tests 7 and 8 addressed the effects of long-term heat sinks, and helium addition to simulate hydrogen from postulated severe accidents. These tests were used to validate the computer code's ability to predict helium or hydrogen concentration during a postulated severe accident. After the system has come to steady-state with a constant steam flow rate (Test 7 corresponds to this steady-state condition), the helium is injected at a constant flow rate for 30 minutes and the system is allowed to achieve a second steady-state (Test 8 corresponds to this steady-state condition plus the helium-addition transient). The objectives of Tests 7 and 8 are to evaluate long-term heat sinks on non-condensible distribution and to validate the computer code's ability to predict helium or hydrogen concentration during a postulated severe accident.

C. Numerical Results and Their Comparisons with LST

All numerical results obtained from COMMIX-1D code were based on the analytical model as outlined in Sec. II and these results will be compared with the experimental data of LST. In all analyses of Tests 1-8, the turbulent free convection correlation as shown in Eq. 2.37b was used for inside the containment vessel, and the turbulent forced convection correlation as shown in Eq. 2.37c was used for the annulus, except for Test 5, which operated under free convection. After carefully examining the velocity field in annulus of Test 5, we decided to use the turbulent free convection instead of the laminar free convection correlation. Mass transfer is based on heat and mass analogy as outlined in Eqs. 2.38a and 2.38b. Turbulent diffusivity is computed according to the k-ε two-equation turbulence model.

Caution must be exercised in comparison between predicted and measured temperature for the test cases with dry strips. Because we do not know the precise location and size of dry strips in the liquid film, the measured temperature could be higher if a thermocouple is in or next to a dry strip. On the other hand, the measured temperature could be lower if a thermocouple located on a wet surface or next to a the liquid film. A meaningful comparison between predicted and measured temperature is not possible unless the area under consideration is either all wet or all dry. Furthermore, both condensation and evaporation processes are statistical in nature because they are very sensitive to local surface conditions. Also, a uniform thickness and velocity of the local liquid film at the outside of containment vessel is very difficult to maintain at a given elevation. All these uncertainties will be reflected in local temperature measurements. For detailed comparisons of calculated and measured temperature, Test 1 was chosen. This is because there are no dry strips for Test 1.

Because of a large amount of information generated from the comparisons between calculated and measured data, it is not possible to present all information here. However, some essential and meaningful comparisons are presented below:

Fig. 6a, 6b, and 6c are velocity, normalized temperature, and steam mass fraction distribution at J = 4 in Test 1. Unless otherwise noted, the normalized temperature is defined as

$$T_{normalized} = \frac{T - T_I}{T_S - T_I},$$

where T_I is the temperature of the water applied on the outside of the upper dome, and
T_S is the temperature of the steam inlet at the bottom of the vessel.

Streamwise variations of condensate and evaporating liquid film thickness at J = 4 of Test 1 are presented in Fig.7. Figure 8 shows streamwise normalized temperature distributions of condensate and evaporating liquid film on inside and outside surfaces of the containment vessel wall at J = 4 of Test 1.

Figures 9, 10, and 11 present normalized circumferential wall temperature distributions on the inside surface of the containment vessel wall at levels A, C, and E, respectively, and their comparisons between measurements and calculations of Test 1. Levels A, C, and E represent elevations, respectively, at the top, middle, and bottom of cylinder of the containment vessel. Azimuthal angles are marked in Fig. 5. Normalized temperature distribution of moist air in the annulus at various elevations and their comparisons between measurements and calculations of Test 1 are presented in Fig. 12. The normalized temperature for the moist air in annulus is defined as T/T_{in}, where T is the local temperature of the moist air and T_{in} is the inlet air temperature. Figures 13 and 14 show, respectively, condensation and evaporation rate and their comparisons between measurements and calculations of all tests. Similar information of air partial pressure and containment pressure of all tests are shown in Figs. 15 and 16, respectively. Figure 17 shows transient pressure distributions of Tests 6 and 8 and their comparisons with experimental data. The transient pressures are normalized to the steady-state measured pressures, respectively, of Tests 5 and 7.

IV. DISCUSSION AND CONCLUSIONS

- The velocity fields of the gaseous (vapor/air) mixture inside the containment vessel and in the annulus are shown in Fig. 6a. Inside, the streamwise flow along and in close proximity of the vertical wall is downward. In the upper central region of the containment vessel, the mixture generally flows upward. There are two distinct recirculatory flows, as predicted, occuring in a major portion of containment vessel; one under the dome and the other over the entire containment vessel. The flow fields in the upper and lower dome region are vastly different from those in the cylindrical region. In addition to the complexity of the flow field, the mixture is highly stratified. Temperature is higher in the top portion of the containment vessel than in the lower portion (see Fig. 6b), and more steam is at the top than the bottom of the vessel because air is heavier than steam (see Fig. 6c). In the exterior annulus, the bulk of the flow is upward, and the flow is turbulent when the draft fan located at the top of annulus is operating (see Figure 6a). Note that the flow field as shown in Fig. 6a is for the PCCS away from the close proximity of a vertical plane passing through a break floor during a postulated DBA.

- Figure 7 shows the calculated streamwise variations in the thickness of the condensate and evaporating liquid film. Filmwise condensation is assumed and agrees reasonably well with experimental observation. Condensate film thickness drops to zero when it hits a gutter. The thickness of the evaporating liquid film depends on the evaporation rate and on the cooling water flooding rate. In principle, the flooding rate could be kept at a minimum, consistent with the requirement that the vessel surface be completely covered or be covered to a maximum extent. A thickness that greatly exceeds the minimum is undesirable because it unnecessarily increases the overall resistance to heat transfer and wastes precious water inventory.

- The steam/air flow inside the containment vessel during a DBA produces mixed convection. At present, the understanding of transition from laminar to turbulent flow in mixed-convection boundary layers is far from satisfactory. For this reason, it was decided as a first step to consider the boundary layer flow to be turbulent for the entire containment vessel wall. Based on our literature survey, very little work has been done in the area of turbulent mixed convection. An analysis of the turbulent mixed convection along a vertical isothermal plate in aiding flow has been reported by Chen et al. We decided to use Chen's correlation on turbulent mixed convection for our analysis,. a choice dictated because a better correlation is not currently available in the open literature. It should be pointed out that Chen's correlation converges to a known result for pure turbulent forced convection but underpredicts the local Nu by approximately 29% for pure free convection. In fact, we obtained very good agreement between COMMIX predictions and experimental data of Westinghouse's PCCS Small Scale Tests (SST) [16] by using Chen's correlation. However, when we use Chen's correlation for LST, the agreement was poor. This is because the forced convection component dominates for SST and the free convection component dominates for LST. Because flow inside the containment vessel is mixed convection, we strongly recommend developing a mixed-convection correlation applicable to the entire range from forced to free convection dominating flows.

- Careful examination of the predicted fluid temperature distribution in the air annulus for most of the LST reveals that the predicted outlet temperatures are consistently lower than the corresponding measured temperatures, and yet the predicted fluid temperatures along the air annulus from the inlet to diffuser are somewhat overpredicted as compared with the measured temperatures (see Fig. 12) for Test 1. Based on experimental observation, fog formed preferentially above the upper dome region. It is our contention that the fluid outlet temperature in the air annulus will be

higher if the effect of the fog is properly accounted for. Additional modeling work, as well as additional experimental measurements, to quantity fog formation is needed.

- In the COMMIX simulation model, all dry strips on the outside vessel surface are combined into one or several circumferential sectors. Thus, the COMMIX calculated vessel wall temperatures in the dry sector are higher than the corresponding measured wall temperatures. A higher vessel wall temperature will reduce the condensation rate. For a given condensation rate, an increasing steam concentration is necessary to compensate for the reduced condensation rate due to higher wall temperature. Thus, containment vessel pressure increases.

- We compute turbulent diffusivity based on the k-ε two-equation turbulent model. From the comparison between COMMIX predictions and air partial pressure data, it appears that we overpredicted flow stratification and underpredicted turbulent diffusivity. This is because buoyancy, in general, tends to decrease turbulent mixing and thus it increases turbulent diffusivity.

- In developing the liquid-film tracking model, the formulation can be simplified greatly if we neglect both the inertia and convective terms in the momentum equation. The justifications for such simplification appear reasonable for applications of the liquid film tracking model under consideration. The inertia effect is characterized by a time scale $\rho\delta^2/\mu$. This is the time needed to approach a steady-state velocity following a disturbance. For a water film of thickness of approximately 0.1-1.0 mm, the characteristic time scale at room temperature is approximately 0.01-1.0 s. Thus, the inertia effect is not significant if the time scale of the imposed disturbance is much greater than 0.01 to 1.0 s. The convective effect can be estimated from known results for parallel flow past a flat plate. For a vertical film of thickness δ, a disturbance at its free surface will penetrate a layer of certain thickness at a distance x downstream. This thickness is roughly $5(\mu x/\rho\bar{u})^{1/2}$, where $\bar{u}$ is the mean flow velocity. If one assumes a parabolic velocity distribution for the film flow, the distance x for the disturbance to reach the entire thickness δ is $0.013\ \rho^2 g\delta^4/\mu^2$. For a room-temperature water film of thickness 0.1-1.0 mm, x is 0.13 to 130 mm. The distance will be shorter for inclined layers. The cited range will be different if velocity distributions other than parabolic are assumed, but the order of magnitude will remain unchanged. Thus, in view of the large longitudinal dimensions of the containment vessel, neglect of the convective effect would not seriously influence the fluid dynamics of the condensate film flow.

- It is well known that the most efficient way to remove heat is by phase change. The PCCS utilizes phase change, (condensation and evaporation) to remove DBA generated heat during a DBA from the containment vessel to the environment via natural circulation. At first glance, the modeling of PCCS is a two-phase problem. If one carefully examines the physical phenomena occurring in the PCCS and judiciously chooses computational domains, it is possible that the formulation can be greatly simplified by reducing the two-phase problem into a single phase with multicomponents. The rates of both condensation and evaporation can be treated as boundary conditions that can be updated iteratively from the temperatures of the bulk gaseous mixture and liquid film surface temperature. The advantages of this novel formulation are that both the convergence problem and long computer running time encountered in the two-phase flow problems can be avoided.

- Based on the comparisons between results obtained from COMMIX code and experimental data of LST, as shown in Figs. 9-17, agreement is good. We are very encouraged and gratified that the maximum error in containment pressure, $(P_p - P_m)/P_m$, is no more than 14% for all LSTs been analyzed (where P_p and P_m are predicted and measured pressure, respectively), and that the maximum local wall temperature difference throughout the containment vessel is less than 13°C for the LST with 100% water coverage on the outside surface of the containment. Similar agreement for the Westinghouse small-scale tests (SST) [16] was also obtained with the identical simulation model used for the LST. Additional validation with pertinent experimental data, as well as refinements of the current simulation model used in the COMMIX-1D code, will further enhance confidence in scaling up to AP-600 PCCS. Nevertheless, we have clearly demonstrated that the COMMIX-1D code can be used to predict the performance of AP-600 PCCS.

ACKNOWLEDGMENTS

The authors want to thank Mr. Allen Notafrancesco and Dr. Alan Rubin of the Division of System Research, Office of Nuclear Regulatory Research, U. S. Nuclear Regulatory Commission, for their support. Cooperation received from Nuclear and Advanced Technology Division of Westinghouse Electric Corporation is also acknowledged.

REFERENCES

1. W. T. Sha, H. M. Domanus, R. C. Schmitt, J. J. Oras, and E. I. H. Lin, *COMMIX-1: A Three-Dimensional Transient Single-Phase Computer Program for Thermal-Hydraulic Analysis*, NUREG/CR-0785, Argonne National Laboratory Report ANL-77-96 (Sept. 1978).

2. H. M. Domanus, R. C. Schmit, W. T. Sha, and V. L. Shah, *COMMIX-1A: A Three-Dimensional Transient Single-Phase Computer Program for Thermal-Hydraulic Analysis of Single and Multicomponent Systems*, Vol. I User's Manual, and Vol. II Assessment and Verification, NUREG/CR-2896, Argonne National Laboratory Report ANL-82-25 (Dec. 1983).

3. F. F. Chen, H. M. Domanus, C. C. Miao, R. C. Schmitt, V. L. Shah, and W. T. Sha, *COMMIX-1B: A Three-Dimensional Transient Single-Phase Computer Program for Thermal-Hydraulic Analysis of Single and Multicomponent Systems*, Vol. I Equations and Numerics, and Vol. II User's Manual, NUREG/CR-4348, Argonne National Laboratory Report ANL-85-42 (Sept. 1985).

4. H. M. Domanus, Y. S. Cha, T. H. Chien, R. C. Schmitt, and W. T. Sha, *COMMIX-1C: A Three-Dimensional Transient Single-Phase Computer Program for Thermal-Hydraulic Analysis of Single and Multicomponent Engineering Systems*, Vol. I Equations and Numerics, and Vol. II User's Manual, NUREG/CR-5649, Argonne National Laboratory Report ANL-90-33 (Sept. 1990).

5. T. H. Chien, W. T. Sha, and J. G. Sun, *COMMIX-1D: A Three-Dimensional Transient Single-Phase Multicomponent Computer Program for Thermal-Hydraulic Analysis of Reactor Containment*, To be published, 1996.

6. W. T. Sha, B. T. Chao, and S. L. Soo, *Local Volume-Averaged Transport Equations for Multiphase Flow in Regions Containing Distributed Solid Structures*, NUREG/CR-2354, Argonne National Laboratory Report ANL-81-69 (Dec. 1981).

7. B. E. Launder and D. B. Spalding, *Lectures in Mathematical Models of Turbulence*, Academic Press (1972).

8. W. T. Sha and B. E. Launder, Argonne National Laboratory, unpublished information (1979).

9. B. E. Launder, G. J. Reese, and W. Rodi, *Progress in the Development of a Reynolds-Stress Turbulent Closure*, J. Fluid Mech. 68, pp. 537-566 (1975).

10. V. S. Arpaci and P. S. Larsen, *Convective Heat Transfer*, Prentice-Hall, Englewood Cliffs, NJ (1974).

11. B. E. Launder, A. Morse, W. Rodi, and D. B. Spalding, *The Predication of Free Shear Flowss - A Comparison of the Performance of Six Turbulent Models*, Proc. NASA Langley Working Conf. on Free Turbulent Shear Flows, NASA SP-321, (1972).

12. E. Boltz, *Grenzschichten an Rotationskopern*, Doctorate Dissertation, University of Gottingen, Germany (1908).

13. H. Schlichting, *Boundary-Layer Theory*, 7th Ed., p. 235, McGraw-Hill (1978).

14. K. E. Washington et al. Reference *Manual for the CONTAIN 1.1 Code for Containment Severe Accident Analysis*, Report NUREG/CR-5715 (SAND-91-0835), July 1991.

15. T. S. Chen, B. F. Armaly, and M. M. Ali, *Turbulent Mixed Convection Along A Vertical Plate*, J. Heat Transfer, 109: 251-253 (1987).

16. J. G. Sun, T. H. Chien, J. Ding, and W. T. Sha, *Validation of COMMIX With Westinghouse AP-600 PCCS Test Data, Nuclear Safety*, Vol. 36. No. 2 (July-Dec., 1995).

17. Private Communication with Westinghouse Staff, 1995.

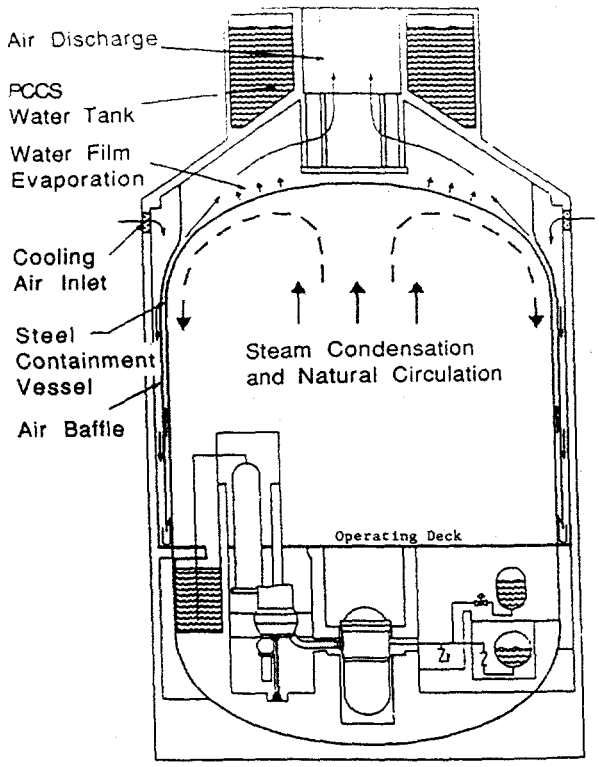

Fig. 1. AP-600 Passive Containment Cooling System

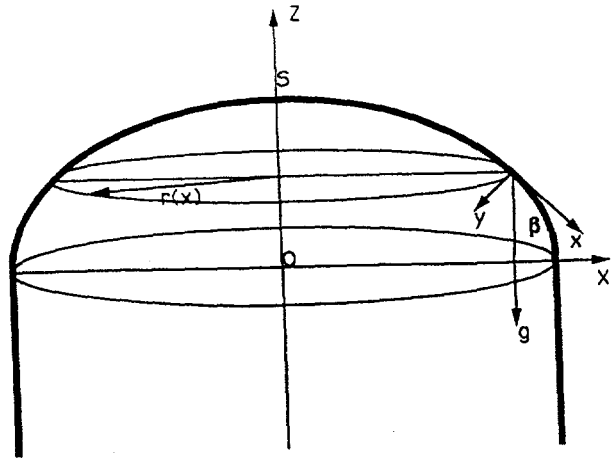

Fig. 2. Curvilinear Coordinates (x,y) Associated with Meridional Section of Elliptical Dome

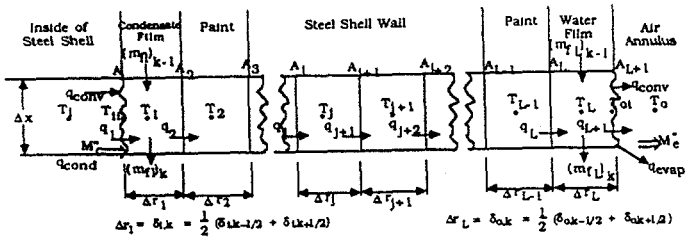

Fig. 3. Discretization Scheme of Thermal Coupling Domain (Domain 3)

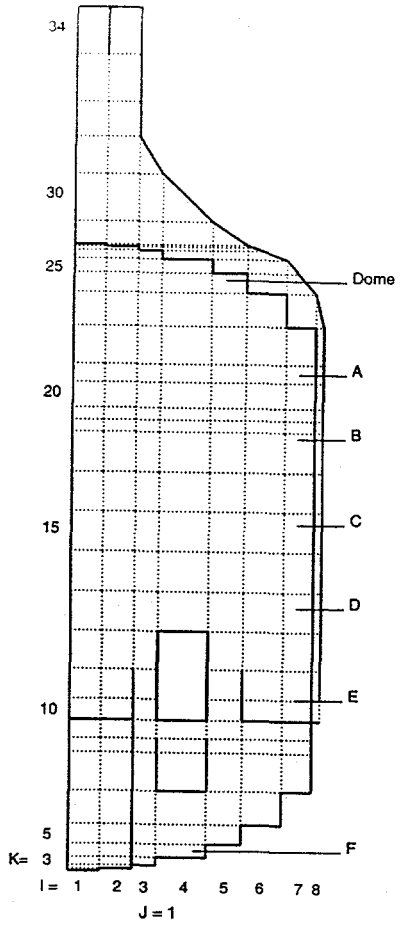

Fig. 4. Computational Mesh Representation for LST on R-Z Cross Section

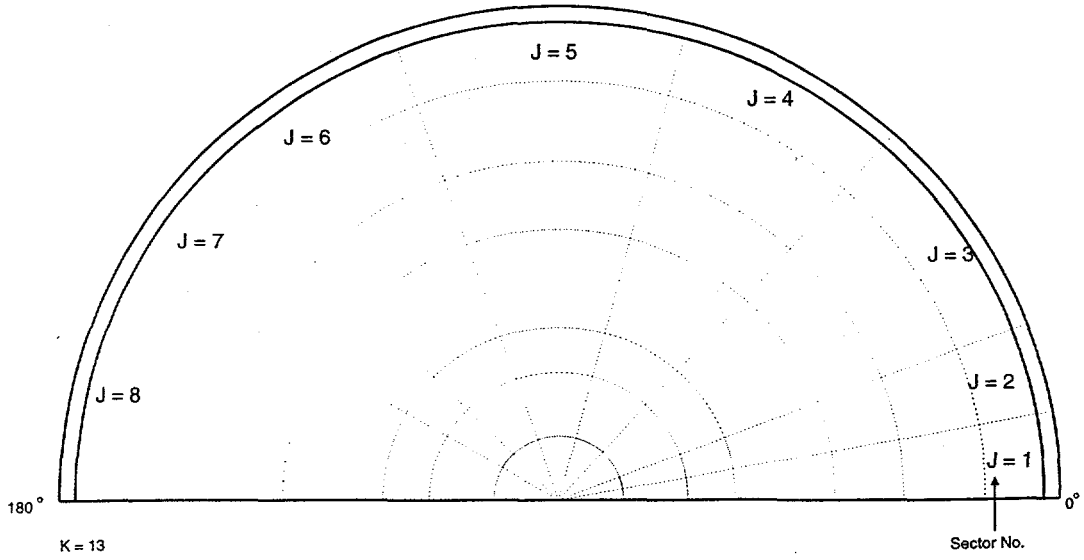

Fig. 5. Computational Mesh Representation for LST on R-θ Cross Section with J_{max} = 8

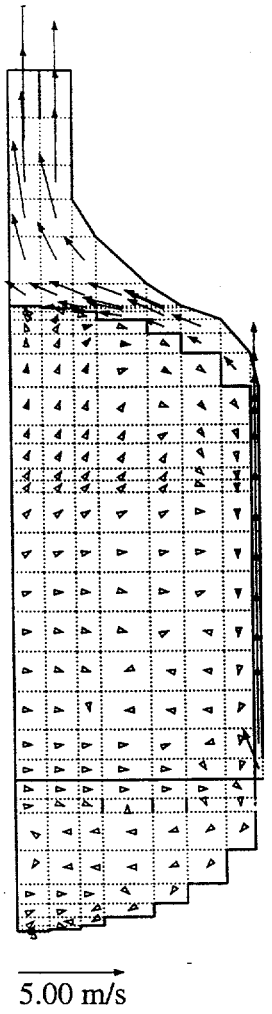

Fig. 6a. Velocity Distribution at J = 4 of Test 1

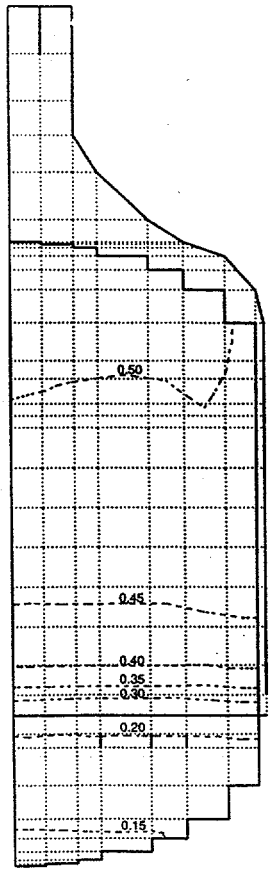

Fig. 6b. Normalized Temperature Distribution at J = 4 of Test 1

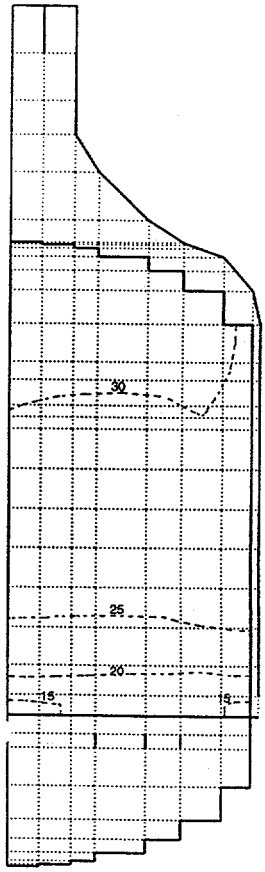

Fig. 6c. Steam Mass Fraction (%) Distributio at J = 4 of Test 1

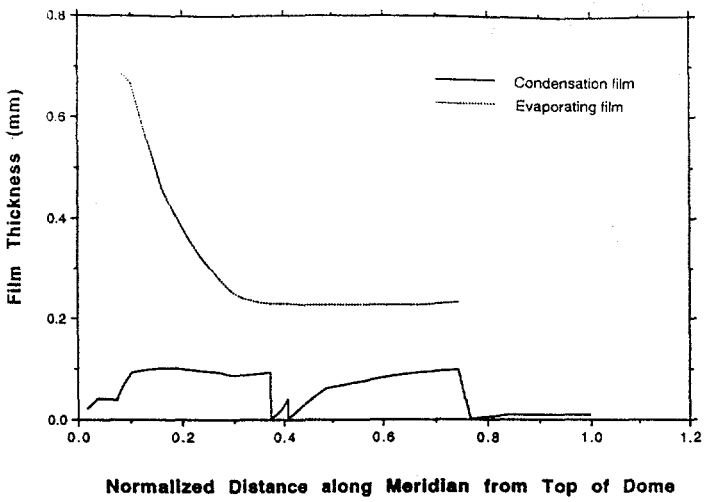

Fig. 7. Streamwise Variations of Condensate and Evaporating Film Thickness at J = 4 of Test 1

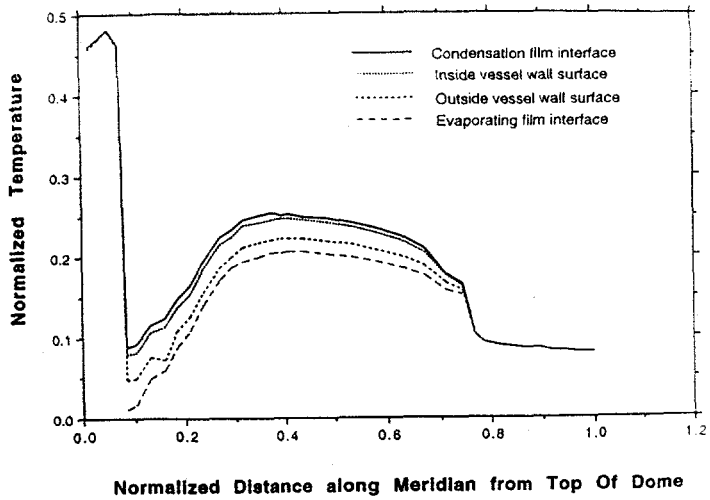

Fig. 8. Streamwise Normalized Temperature Distributions of Inside and Outside Vessel Wall Surface, Condensation and Evaporating Film Interface

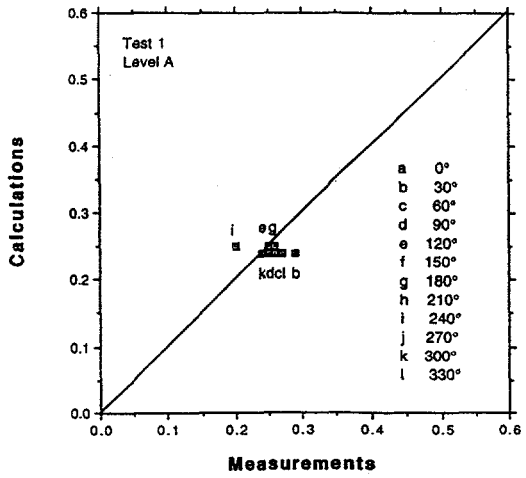

Fig. 9. Calculated and Measured Normalized Circumferential Wall Temperature Distribution of Inside Surface at Top of Cylindrical Vessel of Test 1

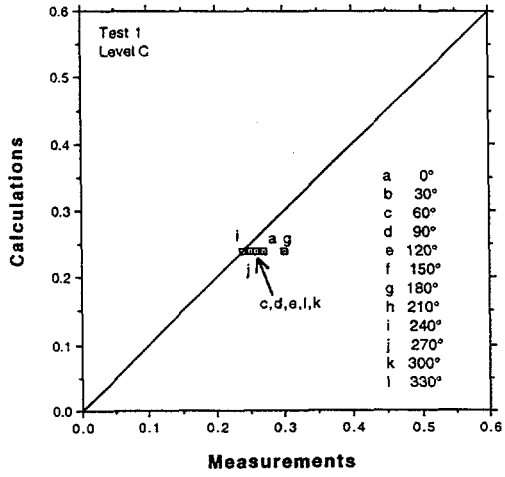

Fig. 10. Calculated and Measured Normalized Circumferential Wall Temperature Distribution of Inside Surface at Middle of Cylindrical Vessel of Test 1

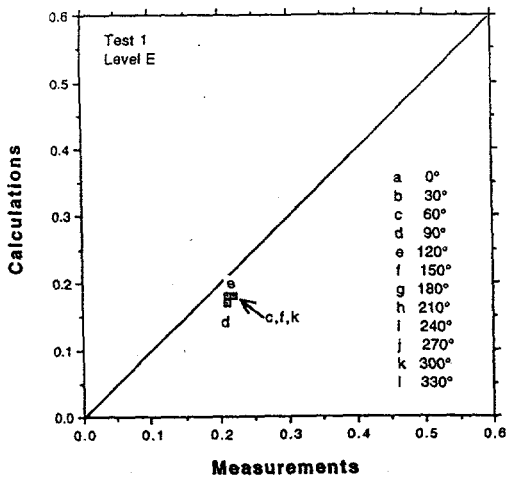

Fig. 11 Calculated and Measured Normalized Circumferential Wall Temperature Distribution of Inside Surface at Bottom of Cylindrical Vessel of Test 1

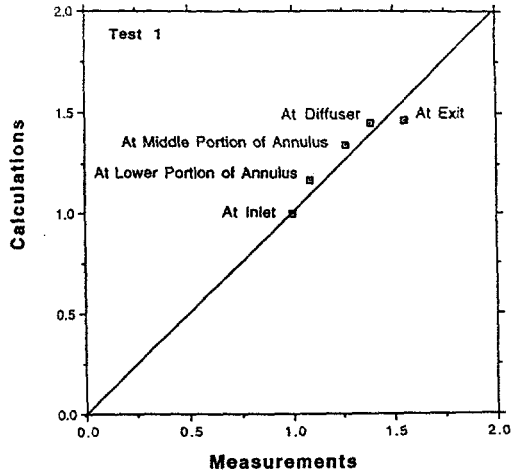

Fig. 12. Calculated and Measured Normalized Temperature Distribution of Moist Air in Annulus at Various Elevations of Test 1

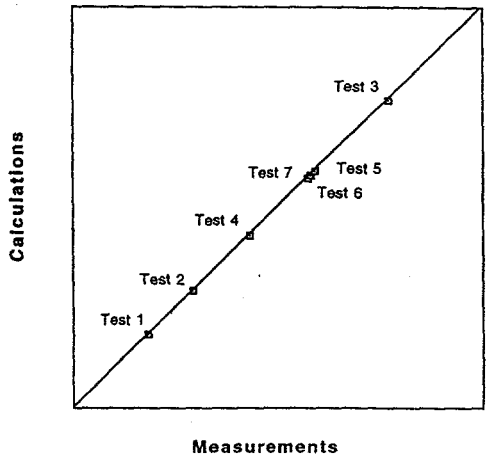

Fig. 13. Calculated and Measured Condensation Rate

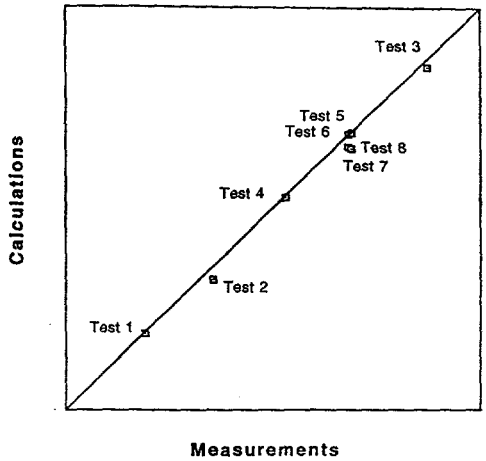

Fig. 14. Calculated and Measured Evaporation Rate

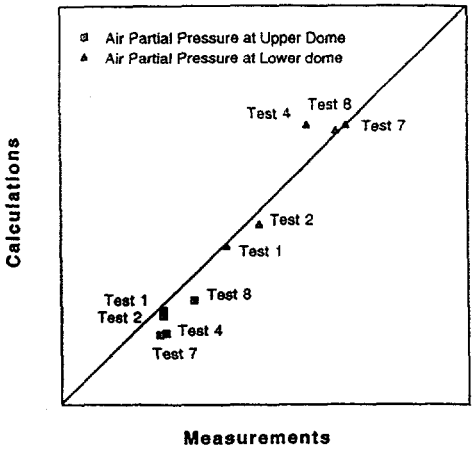

Fig. 15. Calculated and Measured Air Partial Pressure at Upper and Lower Dome

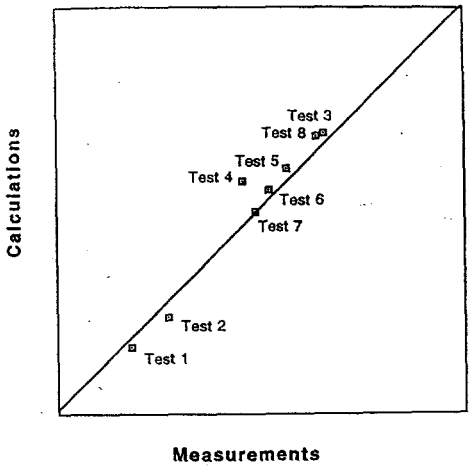

Fig. 16. Calculated and Measured Containment Pressure

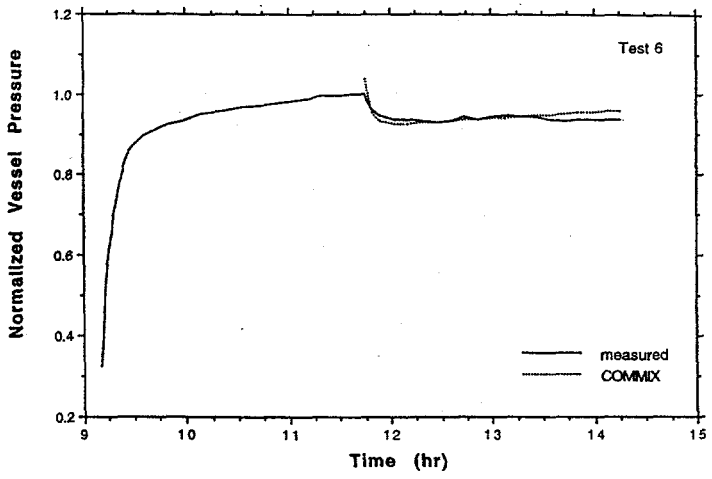

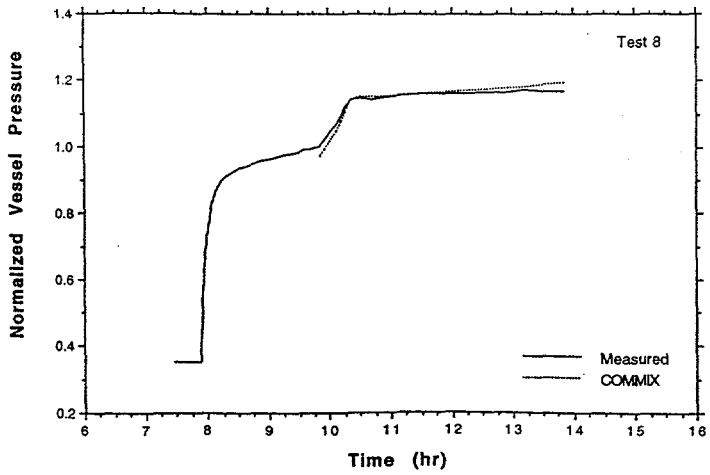

Fig. 17. Calculated and Measured Normalized Containment Pressure during Transient Tests 6 and 8